Geophysical Research Letters

RESEARCH LETTER
10.1029/2021GL097605

Key Points:

- Long-lived active dune fields are in apparent contradiction with the predicted rapid abrasion of windblown organic sediment on Titan
- Episodic abrasion and sintering of organic sediment, driven by seasons, could generate sand with equilibrium sizes on Titan
- Titan's undifferentiated plains and labyrinth terrains could result from prolonged sintering and diagenesis where transport is infrequent

Supporting Information:

Supporting Information may be found in the online version of this article.

Correspondence to:

M. G. A. Lapôtre,
mlapotre@stanford.edu

Citation:

Lapôtre, M. G. A., Malaska, M. J., & Cable, M. L. (2022). The role of seasonal sediment transport and sintering in shaping Titan's landscapes: A hypothesis. *Geophysical Research Letters*, *49*, e2021GL097605. https://doi.org/10.1029/2021GL097605

Received 22 DEC 2021
Accepted 25 MAR 2022

Author Contributions:

Conceptualization: Mathieu G. A. Lapôtre
Data curation: Mathieu G. A. Lapôtre, Michael J. Malaska, Morgan L. Cable
Formal analysis: Mathieu G. A. Lapôtre, Michael J. Malaska, Morgan L. Cable
Investigation: Mathieu G. A. Lapôtre
Methodology: Mathieu G. A. Lapôtre
Project Administration: Mathieu G. A. Lapôtre
Resources: Mathieu G. A. Lapôtre
Visualization: Mathieu G. A. Lapôtre

The Role of Seasonal Sediment Transport and Sintering in Shaping Titan's Landscapes: A Hypothesis

Mathieu G. A. Lapôtre[1], Michael J. Malaska[2], and Morgan L. Cable[2]

[1]Department of Gelogical Sciences, Stanford University, Stanford, CA, USA, [2]Jet Propulsion Laboratory, California Institute of Technology, Pasadena, CA, USA

Abstract Titan is a sedimentary world, with lakes, rivers, canyons, fans, dissected plateaux, and sand dunes. Sediments on Saturn's moon are thought to largely consist of mechanically weak organic grains, prone to rapid abrasion into dust. Yet, Titan's equatorial dunes have likely been active for 10s–100s kyr. Sustaining Titan's dunes over geologic timescales requires a mechanism that produces sand-sized particles at equatorial latitudes. We explore the hypothesis that a combination of abrasion, when grains are transported by winds or methane rivers, and sintering, when they are at rest, could produce sand grains that maintain an equilibrium size. Our model demonstrates that seasonal sediment transport may produce sand under Titan's surface conditions and could explain the latitudinal zonation of Titan's landscapes. Our findings support the hypothesis of global, source-to-sink sedimentary pathways on Titan, driven by seasons, and mediated by episodic abrasion and sintering of organic sand by rivers and winds.

Plain Language Summary Like Earth, Saturn's moon Titan hosts lakes, rivers, canyons, fans, eroded plateaux, and sand dunes. On Titan, loose solid particles (or sediments) are likely made of soft hydrocarbon grains, prone to rapid breakdown into dust. Yet, Titan's equatorial dunes have been active for up to several hundreds of thousands of years, suggesting that some mechanism must produce sand-sized particles at these latitudes. We explore the hypothesis that a combination of abrasion, when grains are transported by winds or methane rivers, and sintering, when they are at rest, could produce sand grains that maintain an equilibrium size. Our model demonstrates that seasonal sediment transport could produce sand on Titan and could explain the distribution of Titan's landscapes. Altogether, our findings support the hypothesis of global sedimentary pathways on Titan, driven by seasons, and mediated by episodic abrasion and sintering of organic sand by rivers and winds.

1. Introduction

Alongside Earth and Mars, Titan is the third planetary body in the solar system to show evidence for widespread and diverse sedimentary environments, including lakes (Hayes, 2016), rivers (Langhans et al., 2012), alluvial fans or deltas (Birch et al., 2016), eroded canyonlands (Poggiali et al., 2016), dissected plateaux (Malaska et al., 2020), and sand dunes (Lorenz, Wall et al., 2006). The latitudinal distribution of Titan's terrains, with sand dunes largely concentrated around the moon's equatorial belt, undifferentiated plains at mid-latitudes, and labyrinth terrains and lakes near the poles (Lopes et al., 2020), suggests a strong control of climate on Titan's surface processes and landscape formation (Figure 1a). Climate models predict that Titan's single-celled, pole-to-pole Hadley circulation splits into two cells as atmospheric circulation reverses near equinox (Hörst 2017), possibly leading to intense mid-latitude and equatorial storms that drive significant sediment transport by winds and rivers. Global circulation model (GCM) predictions (Charnay et al., 2015; Tokano, 2008, 2010), combined with models for eolian transport (Burr et al., 2015; Comola et al., 2022; Kok et al., 2012), reveal that winds capable of transporting dune sands typically occur ~0.1%–10% of the time at all latitudes (similar to or possibly lower than transport intermittency on Earth; e.g., Comola et al., 2019; see also Comola et al., 2022). Except for two equinox storms, equatorial winds are relatively steady throughout the year, whereas sand transport may occur through infrequent but strong wind gusts at higher latitudes (Figure S1 in Supporting Information S1). In addition to models, 13 years (or a little less than half a Titan year, which is ~29.4 Earth years) of episodic Titan flybys by Cassini revealed that the moon's methane cycle includes methane rainstorms and even inundation (Barnes et al., 2013; Turtle et al., 2011), with more storms near the poles (~100 storms per season) than near the equator (<1 storm per season; Hayes et al., 2018). Despite the relative infrequency of equatorial storms, surface changes (Barnes et al., 2013; Turtle et al., 2011) and dust plumes (Rodriguez et al., 2018) were detected near equinox.

Writing – original draft: Mathieu G. A. Lapôtre
Writing – review & editing: Mathieu G. A. Lapôtre, Michael J. Malaska, Morgan L. Cable

Assuming that each storm lasts for 1–10 hr (Hayes et al., 2018), rainstorm intermittency is <~0.4% near the poles and <~0.004% near the equator. Images acquired by the Huygens lander support the hypothesis of recent intermittent surface flows near the equator, showing fine (< a few millimeters in diameter) dark grains, including sand-sized (Zarnecki et al., 2005) organic grains (Tomasko et al., 2005), surrounding few decimeter-scale rounded clasts, interpreted as fluvially transported cobbles on a dry riverbed (Tomasko et al., 2005; Figures 1b and 1c). Furthermore, the morphology and crestline orientations of Titan's equatorial dunes suggest that they have been responding to orbitally forced changes in environmental conditions—and thus have been active—over the recent past (10s–100s kyrs, or ~3,000–45,000 Titan years; Ewing et al., 2015). Ongoing dune formation is further supported by the presence of compositionally distinct interdune areas (Barnes et al., 2008; Bonnefoy et al., 2016). Thus, models and spacecraft observations indicate that seasonal, active sediment transport shapes the modern landscapes of Titan.

From saltation mechanics, we know that grain sizes within dune fields should be relatively narrowly distributed, and on Titan, are predicted to be around 150–300 μm in diameter (Burr et al., 2015; Kok et al., 2012), although slightly finer or coarser grains may be permitted if dune materials were cohesive (e.g., Comola et al., 2022; Lorenz, 2017). Finer grains are more prone to stabilizing interparticle interactions (possibly including triboelectric charging; Mendéz Harper et al., 2017) that raise the wind speed required to mobilize them; in turn, coarser grains are heavier and thus also harder to move. Several mechanisms have been proposed to generate sand on Titan, such as the erosion of lithified materials, sintering of photochemically produced airfall particles, flocculation, and erosion of evaporitic precipitates (Barnes et al., 2015). On Earth, large dune fields are typically supplied with pre-sorted sediments from fluvial or coastal sands or sandstones (Busch, 2020; Lancaster, 1982; Pastore et al., 2021) as rivers, waves, and winds efficiently sort sediments by grain size and density (e.g., Goosmann et al., 2018; Jerolmack et al., 2011; Komar, 2007; Parker, 1991). On Earth, abrasion of mechanically weak evaporitic minerals is known to occur during eolian transport (Jerolmack et al., 2011). The source of sand on Mars is unclear (e.g., Tirsch et al., 2011) but sedimentary recycling is known to occur (Edgett et al., 2020), and many ancient fluvial outcrops could supply pre-sorted sand-sized materials (Dickson et al., 2020). Furthermore, basaltic grains are mechanically strong (Yu et al., 2018) such that Martian winds themselves could have sorted sands over billion-year timescales. In contrast, laboratory experiments suggest that the organic materials thought to make up Titan's dune sand (Barnes et al., 2008; Lorenz and Lunine, 1996) are mechanically weak (Yu et al., 2018). This suggests that dune sand should be highly susceptible to comminution (fining through abrasion) during eolian transport on Titan—an apparent paradox that has led to the hypotheses that either transport is of commensurate low energy (Lorenz and Lunine, 1996) or that Titan's dune sand is derived locally (Barnes et al., 2015; Yu et al., 2018).

Here, we first explore the hypothesis that Titan's dune sand is fining through time due to progressive abrasion, but that the dunes have been able to persist over 10s–100s kyrs without local sand replenishment because eolian abrasion is slow. Next, we consider the alternative hypothesis that, even though abrasion leads to fining and dust production, grain comminution during transport is compensated by coarsening through grain sintering (i.e., coalescence of fine grains into coarse grains when sediments are not transported; Herring, 1950; Barnes et al., 2015), permitting the continuous production of relatively well-sorted equilibrium sand sizes within Titan's dunes over geologic timescales. Finally, we discuss potential implications of our model results for the genesis of Titan's landscapes.

2. Methods

2.1. Equilibrium Grain Size Produced by Intermittent Transport and Sintering

We consider the abrasion model of Trower et al. (2017) for the abrasion of individual particles during fluvial transport (Section 2.2). Fluvial abrasion in both bedload and suspended load is modeled for individual impacting organic grains experiencing fluvial sediment transport in a stream of 80% CH_4 – 20% N_2 liquid (Hayes, 2016; Malaska et al., 2017; Section 2.2). As abrasion rate varies with particle impact velocity, we consider typical flow conditions as constrained from a combination of data acquired by the Huygens probe during its descent and upon landing. Eolian abrasion is then modeled by scaling fluvial abrasion rates to account for the different fluid properties and for typical eolian saltation trajectories on Titan (Kok et al., 2012; Figure 2a; Section 2.3). This approach is justified because, owing to Titan's thick atmosphere, windblown sand transport is expected to be more akin to sand transport by water on Earth than by air on Earth and Mars, with minimal importance of grain splash (Kok et al., 2012) unless sand is highly cohesive (Comola et al., 2022). In the case of cohesive sediments, our scaling relationship for eolian abrasion rates still provides a first-order estimate of abrasion rate for the saltating grain

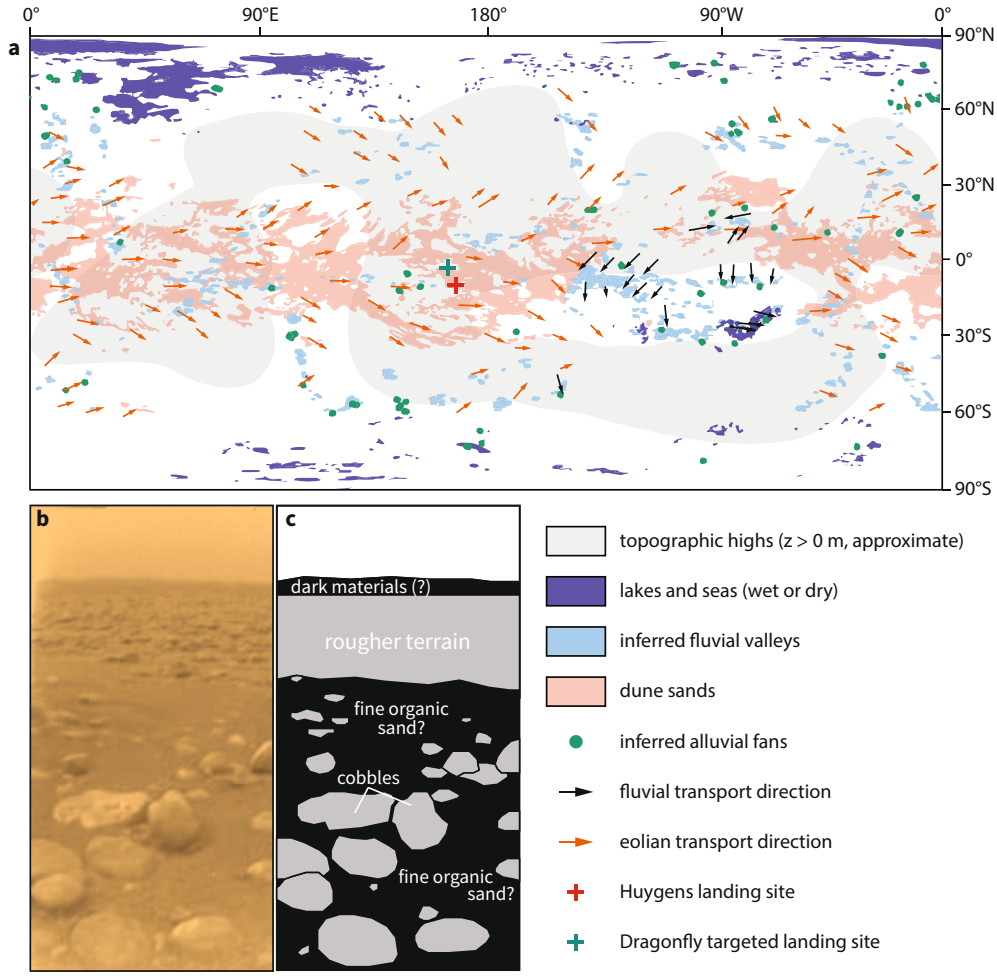

Figure 1. (a) Sedimentary pathways on Titan as inferred from Cassini data. Dune sands, lakes, and seas were mapped by Lopes et al. (2020), alluvial fans by Birch et al. (2016), fluvial valleys and associated flow directions by Burr et al. (2013), and eolian transport directions by Malaska, Lopes, Hayes, et al. (2016). We note that finer-scale features such as fans and valleys could only be mapped along discrete orbital swaths, such that their occurrence is almost certainly much more widespread than depicted here. The eighth-order spherical-harmonic fit to Titan's topography corrected for the geoid of Corlies et al. (2017) was used to provide an indication of Titan's long-wavelength topography, with topographic highs (elevation, z, above 0-m datum) highlighted. The location of the Huygens probe's landing site (b and c) and landing target for the Dragonfly mission (Lorenz et al., 2021; Malaska, Lopes, Williams, et al., 2016) are also shown. (b) Image of the Huygens probe's landing site, acquired by the Descent Imager/Spectral Radiometer instrument aboard the landed spacecraft (image credit: ESA/NASA-JPL/University of Arizona). (c) Annotated sketch of (b), showing large, decimeter-scale cobbles and fine (<2 mm) dark grains in the proximity of the lander. The landing site was interpreted as a dry riverbed covered in fluvially transported sediments (Tomasko et al., 2005).

population, whereas splashed grains would likely experience lower abrasion rates. Finally, the sintering scaling relationship of Herring (1950) was used to predict the time it takes for neighboring particles to sinter into a larger particle (Section 2.4). To account for uncertainty related to material, mechanical, and sintering properties of Titan sediments, wide ranges of parameter values were explored (Table S1 in Supporting Information S1).

Because the history of sand grains is not known—for example, they could have started as fine haze particles that first sintered or cemented into coarser grains (Barnes et al., 2015; Turtle et al., 2011) or as organic bedrock that weathered (Neish et al., 2015) and eroded into clastic sediments (Barnes et al., 2015)—we assume that a supply of sediment available for transport by fluvial and eolian processes was created by some unconstrained mechanism and only consider their subsequent evolution. Specifically, we calculate the instantaneous sintering $\left(\frac{dD}{dt}\Big|_{s}\right)$ and abrasion $\left(\frac{dD}{dt}\Big|_{ab}\right)$ rates of sediment grains (where D denotes grain diameter) subjected to rest or transport, respec-

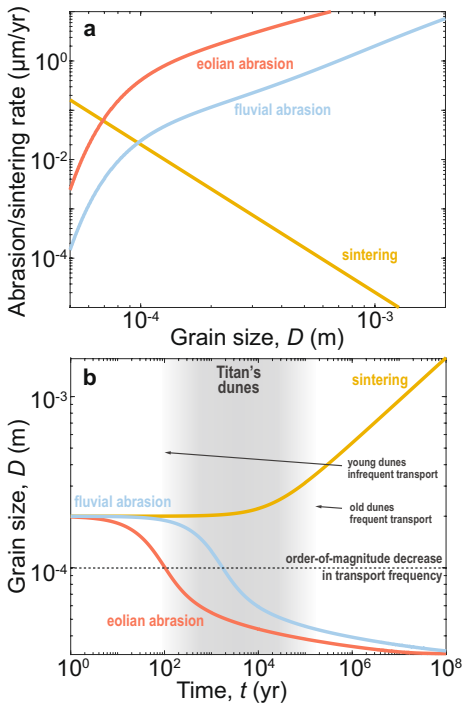

Figure 2. (a) Instantaneous abrasion and sintering rates as a function of sediment-grain diameter on Titan. Whereas sintering rate decreases with increasing grain size, abrasion rates increase owing to increased impact energies. Conversely, impacts of finer grains are viscously damped, producing a sharp drop in abrasion rate for silt-sized grains. (b) Time evolution of an initially 200-μm grain in continuous fluvial (blue) or eolian (orange) transport, and at rest (yellow). Similar results were obtained for starting grain sizes in the 50–2,000 μm range. Shading highlights the duration of continuous transport corresponding to 0.1%–10% intermittent transport over the estimated minimum age of the dune field (i.e., 0.1%–10% of 3,000–45,000 Titan years; Ewing et al., 2015). Rates were computed using our favored set of parameters (Table S1 in Supporting Information S1).

tively (Figure 2). We then solve for transport intermittency (I_t), defined as the fraction of time that individual grains spend in transport, such that

$$\frac{dD}{dt} = (1 - I_t)\left.\frac{dD}{dt}\right|_s + I_t \left.\frac{dD}{dt}\right|_{ab} = 0. \quad (1)$$

Abrasion rate can be further decomposed into fluvial and eolian contributions as

$$\left.\frac{dD}{dt}\right|_{ab} = \left(\frac{I_f}{I_t}\right)\left.\frac{dD}{dt}\right|_{ab,fluvial} + \left(\frac{I_e}{I_t}\right)\left.\frac{dD}{dt}\right|_{ab,eolian}, \quad (2)$$

where I_f and I_e are the intermittencies of fluvial and eolian transport, respectively, such that $I_t = I_f + I_e$. The latter decomposition allows us to explore the effect of variable proportions of fluvial (I_f/I_t) and eolian (I_e/I_t) transport on resulting grain sizes. Sintering parameters and material properties used as input to our model are summarized in Table S1 of Supporting Information S1.

2.2. Abrasion During Fluvial Transport

The model of Trower et al. (2017) predicts the abrasion rate of single grains of diameter, D, during fluvial transport (both bed- and suspended loads) as a function of flow and sediment parameters,

$$\left|\frac{dD}{dt}\right|_{ab,fluvial} = \frac{A}{6}\frac{\rho_s Y w_i^3 D}{k_v \sigma_t^2 H_f} \quad (3)$$

where ρ_s is the sediment density, Y and σ_t are the grain's Young's modulus and tensile strength, respectively, w_i is the grain impact velocity, H_f is the grain's fall height, and $k_v \approx 10^6$ is a dimensionless constant that accounts for differences between particle and bed surface materials (Lamb et al., 2008; Scheingross et al., 2014; Sklar & Dietrich, 2001, 2004; Trower et al., 2017). The dimensionless coefficient, $A \approx 1/3$, accounts for the fact that the time between two consecutive particle impacts onto the bed scales with the sum of the time required to lift the particle from the bed up to a height H_f and the time to settle back onto the bed. Fall height can be calculated from the vertical profile of sediment concentration as

$$H_f = \frac{1}{c_b}\int_{H_b}^{H} z\frac{dc}{dz}dz, \quad (4)$$

where c_b is the near-bed sediment concentration, H is flow depth, H_b is the height of the bedload layer, and z is the elevation above the bed. Suspended sediment concentration, $c(z)$, is determined from a Rouse profile,

$$c(z) = c_b\left[\frac{H_b}{z}\left(\frac{H - z}{H - H_b}\right)\right]^{\frac{w_s}{\beta\kappa u_*}}, \quad (5)$$

where w_s is the sediment settling velocity, u_* is the flow shear velocity, and $\kappa = 0.41$ is the von Kármán constant and β is a coefficient that relates the diffusivities of sediments and momentum. The height of the bedload layer is calculated from sediment transport stage as

$$H_b = 1.44D\left(\frac{\tau_*}{\tau_{*c}} - 1\right)^{1/2}, \quad (6)$$

where τ_* is the Shields number and τ_{*c} its critical value for incipient sediment motion in the bedload.

Impact velocity is calculated following Lamb et al. (2008) as

$$w_i \approx \left[\int_{-w_s}^{6\sigma_w} (w' + w_s)^3 P(w')\, dw'\right]^{1/3}, \tag{7}$$

where $P(w') = \frac{1}{\sqrt{2\pi}\sigma_w}\exp\left(-\frac{w'^2}{2\sigma_w^2}\right)$ is the probability density function of velocity fluctuations, w', and settling velocity, w_s, is calculated using the formulation of Dietrich (1982),

$$w_s = (RgvW_*)^{1/3}, \tag{8}$$

where $R = \frac{(\rho_s - \rho)}{\rho}$ with ρ the fluid density, $W_* = a_1 10^{(a_2+a_3)}$ is a dimensionless settling velocity, and empirical constants a_1, a_2, and a_3 are calculated from dimensionless particle size, $D_* = \frac{RgD^3}{v^2}$, as

$$a_1 = \left[0.65 - \left(\frac{\mathrm{CSF}}{2.83}\tanh(\log(D_*) - 4.6)\right)\right]^{\left(1 + \frac{3.5 - \mathrm{PS}}{2.5}\right)}, \tag{9a}$$

$$a_2 = -3.76715 + 1.92944\log(D_*) - 0.09815(\log(D_*))^2 - 0.00575(\log(D_*))^3 + 0.00056(\log(D_*))^4, \tag{9b}$$

and,

$$a_3 = \log\left(1 - \frac{1 - \mathrm{CSF}}{0.85}\right) - (1 - \mathrm{CSF})^{2.3}\tanh(\log(D_*) - 4.6) + 0.3(0.5 - \mathrm{CSF})(1 - \mathrm{CSF})^2(\log(D_*) - 4.6), \tag{9c}$$

where CSF is the Corey shape factor (CSF = 0.7 for natural grains) and PS is the Powers roundness (PS = 3.5 for natural grains). The model also includes viscous damping, where particle-bed impacts become fully damped at a threshold impact Stokes number of $\mathrm{St} = \frac{Dw_i\rho_s}{9v\rho}$ (Davis et al., 1986; Joseph et al., 2001; Trower et al., 2017).

In an attempt to represent typical fluvial flow conditions on Titan, we assume that the decimeter-scale bright cobbles observed by the Huygens lander are made of water ice and that the coarsest ones (~15 cm in diameter; Burr et al., 2006; Perron et al., 2006; Tomasko et al., 2005) are transported near the threshold of bedload motion to estimate the typical fluid stress, τ_b, imparted by flow on the bed. Combined with bed slope, S, as measured from a recently updated digital elevation model of the Huygens landing site ($S \sim 0.05$; Daudon et al., 2020), we then derive flow depth, h, assuming steady uniform flow conditions (i.e., $\tau_b = \rho ghS$ with $g = 1.35$ m/s^2 the acceleration of gravity). Our calculations are consistent with previous estimates of flow conditions at the Huygens landing site (Burr et al., 2006; Perron et al., 2006). Although the composition of observed bright cobbles is uncertain, we find that an organic rather than water ice composition would decrease estimated flow discharge (and thus estimated abrasion rates) but would not affect our conclusions.

2.3. Abrasion During Eolian Transport

We assume that Equation 3 reasonably applies to windblown saltating grains on Titan, and approximate the rate of eolian abrasion during wind-driven saltation on Titan, for a given grain size, as

$$\left|\frac{dD}{dt}\right|_{ab,eolian} \approx \left(\frac{\alpha^3 w_{s,eolian}^3}{H_{salt}}\right)\left(\frac{H_b}{w_{s,fluvial}^3}\right)\left|\frac{dD}{dt}\right|_{ab,fluvial}, \tag{10}$$

where $\alpha \approx \sin\left(\mathrm{atan}\left(\frac{H_{salt}}{L_{salt}}\right)\right)$ accounts for grain impacts that are non-normal to the bed, with H_{salt} and L_{salt} the typical saltation heights and lengths, respectively, and where impact velocity is assumed to scale with settling velocity, w_s. We used $H_{salt} \sim 8$ mm and $L_{salt} \sim 8$ cm, as estimated by a numerical model (Kok et al., 2012).

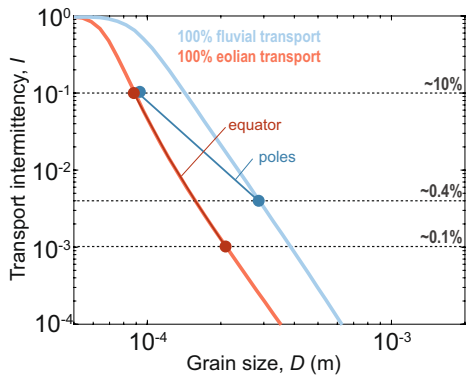

Figure 3. Transport intermittencies required to produce sand-sized equilibrium organic grains on Titan. Thick solid lines correspond to 100% transport by winds (orange) or rivers (blue). Symbols indicate the range of equilibrium grain sizes predicted to form assuming $I_t \sim 0.1$–10% with 100% eolian transport near the equator and $I_t \sim 0.4$–10.4% with 0%–10% eolian and 0.4% fluvial transport near the poles (as constrained by GCMs and Cassini data), respectively. These results correspond to our favored scenario; a sensitivity analysis was performed and revealed that conclusions are robust despite uncertainties related to material properties (Figure S2 in Supporting Information S1).

2.4. Sintering

The time, t, required for a cluster of particles to sinter into a grain of diameter, D, can be calculated as

$$t = \left(\frac{D}{D_0}\right)^n t_0 \tag{11}$$

(Herring, 1950), where t_0 is a known time required for neighboring particles to sinter into a reference grain of diameter D_0, and $n \in [1,4]$ is an exponent that varies with sintering process. This relationship is robust regardless of the specifics of which mechanism actually leads to sintering (viscous or plastic flow, evaporation and condensation, volume diffusion, or surface migration; Herring, 1950). Equation 11 can be rearranged to solve for particle diameter as a function of time,

$$D = D_0\left(\frac{t}{t_0}\right)^{1/n}, \tag{12}$$

such that sintering rate can be obtained by differentiating Equation 12 with respect to time,

$$\left|\frac{dD}{dt}\right|_s = \frac{D_0}{n}\left(\frac{t^{1-n}}{t_0}\right)^{\frac{1}{n}}. \tag{13}$$

Finally, we solve for sintering rate as a function of grain diameter by substituting t from Equation 11 into Equation 13, i.e.,

$$\left|\frac{dD}{dt}\right|_s = \frac{D_0^n D^{1-n}}{nt_0}. \tag{14}$$

Barnes et al. (2008) estimated that it takes a time $t_0 \approx 10^4$–10^8 years to form an organic grain of diameter $D_0 \approx 300$ μm on Titan, and that $n = 4$. Under our hypothesis, equilibrium grains would need to form within shorter timescales than the inferred age of Titan's dunes for the proposed mechanism to supply sediments to, and sustain, the dune field (i.e., $t_0 < 10^6$). However, we explore the full 10^4–10^8 years range reported by Barnes et al. (2008). We note that sintering timescale even shorter than 10^4 years would simply yield coarser equilibrium grains for a given abrasion rate.

3. Results

First, we consider the case of windblown particles subjected to abrasion alone. We find that within the minimum estimated lifespan of Titan's dune fields, 200-μm organic sand grains transported 0.1%–10% of the time by winds would abrade sufficiently to produce fine, harder-to-mobilize grains that would inhibit saltation (Figure 2b). A sensitivity analysis was performed to explore the effect of varying optimal grain size on Titan. We found that only dune fields as young as ~3,000 Titan years (the lower bound on their true age; Ewing et al., 2015) and which experienced highly infrequent transport (<0.1% of the time) would not have experienced significant abrasion (<50% grain size reduction; Figure S1 in Supporting Information S1). Under more realistic scenarios, significant changes in grain sizes are predicted to occur, increasing the saltation threshold and leading to an order-of-magnitude decrease in dune activity. Over time, abrasion would lead to the accumulation of fine dust which could hinder sand transport (e.g., Lapôtre & Rampe, 2018). Thus, it appears probable that some other mechanism must counterbalance the progressive communition of eolian organic sand by abrasion on Titan in order for dunes to have persisted to this day.

Next, we consider the alternative scenario of sediment grains subjected to both abrasion, during fluvial or eolian transport, and sintering, when grains are at rest. Our results (Figure 3) indicate that intermittent grain sintering and transport-driven abrasion are readily able to produce a wide range of equilibrium grain sizes on Titan depending

on transport intermittencies (I_t), including the ~150–300-μm grains thought to make up Titan's equatorial dunes. A sensitivity analysis (Figure S2 in Supporting Information S1) reveals that sand grains at equilibrium consistently form through intermittent transport and sintering despite large uncertainties on sintering-relevant parameters and material properties. Under our favoured scenario (Figure 3), a six-fold decrease in transport intermittency (i.e., transport seven times less frequent) is required to produce 300 μm grains instead of 200 μm grains if all transport occurs in rivers, or a five-fold decrease in transport intermittency (i.e., transport six times less frequent) if all transport occurs by winds, confirming that this process is efficient at producing sandy deposits. For example, 200-μm grains would need to be transported from ~0.15% of the time, if all transport occurred by winds, to ~2% of the time, if all transport occurred in rivers, under our favoured scenario in order to maintain their size through episodic transport. Considering more realistic transport intermittencies as constrained by models and Cassini observations, we find that 90–210 μm sand would form near the equator ($I_t \sim 0.1\% - 10\%$, $\frac{I_e}{I_t} = 100\%$; Figure 3) and 90–300 μm sand near the poles (~90 μm for $I_t = 10.4\%$ and $\frac{I_e}{I_t} = \frac{10}{10+0.4} \approx 96\%$; ~300 μm for $I_t = 0.4\%$ and $\frac{I_e}{I_t} = \frac{0}{0+0.4} = 0\%$; Figure 3). With a relatively higher frequency of methane storms at mid-latitudes (Hayes et al., 2018), more significant ground moisture (Lorenz, Niemann et al., 2006; Tomasko et al., 2005; Williams et al., 2012) may bind sediment grains together, inhibiting eolian transport at higher latitudes, suggesting that sand produced near the poles would likely be coarser than near the equator. Finally, we conducted a sensitivity analysis to explore the impact of sintering parameters (n, t_0) as well as sediment density and tensile strength on equilibrium grain size (Figure S2 in Supporting Information S1), revealing our conclusions to be robust for a variety of parameters except for unlikely combinations of sintering and mechanical properties (with rapidly sintering but mechanically strong grains).

4. Discussion and Conclusion

Episodic abrasion and sintering of organic sediments could explain Titan's latitudinally zoned landscapes (Figure 4). It readily permits the formation of active sand dunes at equatorial latitudes (Figure 4), with some dust production but no significant dust accumulation owing to sintering of dust grains into sand over time. As equatorial winds redistribute sediments toward mid-latitudes (Figure 1a; Malaska, Lopes, Hayes, et al., 2016), ground moisture (Lorenz, Niemann et al., 2006; Tomasko et al., 2005; Williams et al., 2012) may allow for the stabilization of organic sediments, inhibiting eolian transport and promoting sintering, which could lead to the formation over time of indurated deposits that could form Titan's undifferentiated plains (Lopes et al., 2020; Figure 4). This scenario could explain spectral observations of undifferentiated plains compatible with an optical coating of water ice on organic grains caused by surface leaching of exposed materials (Malaska et al., 2020; Solomonodou et al., 2018). Mid-latitude materials may also incorporate dust, primarily produced through abrasion of eolian sand and episodically winnowed out from dune fields during high-wind events (Rodriguez et al., 2018). At higher latitudes, the frequency of fluvial transport increases with the frequency of methane storms, allowing the formation of sand in streams (Figure 4). High-latitude river sand is predicted to be coarser than equatorial dune sand (Figure 3), an effect possibly strengthened by ductile rounding of grains during fluvial transport (Le Gall et al., 2010) rather than brittle failure during eolian transport. When not transported by rivers, coarser organic sand is stabilized by ground moisture, preventing the formation of dunes at high latitudes. As high-latitude sand eventually gets deposited by rivers into local depositional basins, in the presence of soluble cements, it may form widespread organic sandstones via diagenesis as those proposed to compose Titan's dissected labyrinth terrains (Lopes et al., 2020; Malaska et al., 2020; Figure 4).

Given uncertainties related to material properties and fluvial and eolian transport conditions on Titan, other scenarios to explain the longevity of Titan's dunes, such as low-energy sediment transport or local sediment supply, cannot be ruled out with utmost confidence at this time. However, these scenarios appear unlikely given our current knowledge, whereas episodic abrasion and sintering are readily able to explain Titan's latitudinally zoned landscapes. Thus, our model supports the hypothesis of a sedimentary cycle on Titan, driven by seasonal climate forcing, and mediated by episodic sintering and abrasion of organic sand grains by rivers and winds. Sediment grain compositions, shapes, and sizes within the dunes (which may help test the sintering hypothesis) as well as wind speeds, frequencies, and precipitation rates (yielding refined constraints on transport intermittency) will be measured in situ by the Dragonfly mission, slated to land on Titan in the mid-2030s (Barnes et al., 2021; Lorenz et al., 2021). These data, combined with laboratory measurements of material mechanical properties

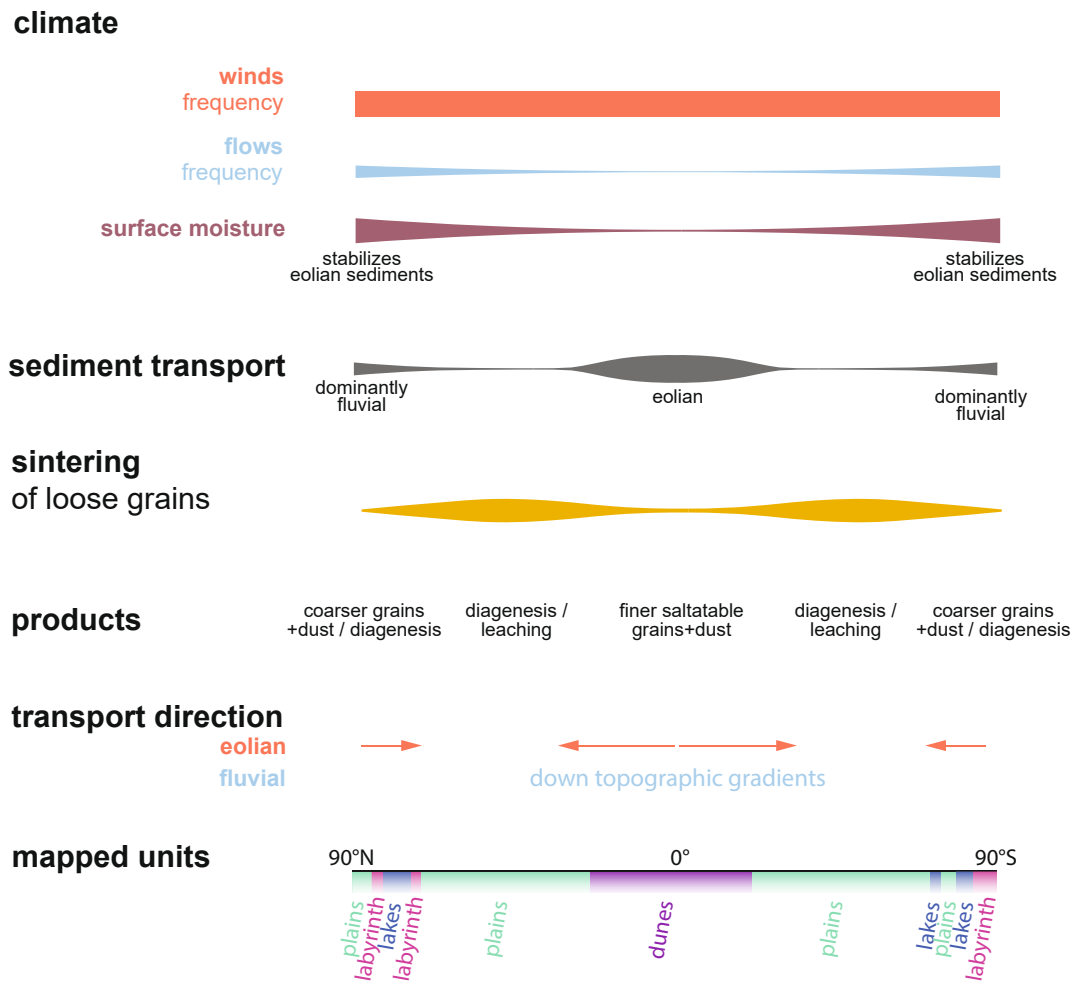

Figure 4. Summary sketch of proposed sedimentary pathways on Titan, whereby a combination of sediment grain abrasion in transport and sintering while at rest produces a supply of sand-sized organic sediments. Under this scenario, more frequent fluvial transport near the poles and eolian transport near the equator would conspire to create dune fields at equatorial latitudes, mid-latitude undifferentiated plains, as well as labyrinth terrains where diagenesis (defined here as chemical and physical changes during and following the induration of sediments into rocks, including recrystallization, but exclusive of breakdown by weathering) may have occurred within sands. The bottom cross-section was simplified from the geomorphologic map of Lopes et al. (2020) and is representative of mapped units along the ~90°E meridian.

(e.g., density, Young's modulus, tensile strength) and sintering rates, will offer a direct test to our hypothesis. If proven correct, our model will in turn provide a key to decipher Titan's recent climate history through the lens of its global source-to-sink sedimentary pathways.

Acknowledgments
We thank Xinting Yu for informative discussions about mechanical properties of Titan-relevant organic materials, and two anonymous reviewers for their constructive comments. This research was supported by a NASA Solar System Workings grant (80NSSC20K0145) awarded to M. G. A. Lapôtre. A portion of this research was carried out at the Jet Propulsion Laboratory, California Institute of Technology, under a contract with the National Aeronautics and Space Administration (80NM0018D0004).

Data Availability Statement

No new data are presented in this manuscript.

References

Barnes, J. W., Brown, R. H., Soderblom, L., Sotin, C., Le Mouélic, Rodriguez, S., et al. (2008). Spectroscopy, morphometry, and photoclinometry of Titan's dunefields from Cassini/VIMS. *Icarus*, *195*, 400–414. https://doi.org/10.1016/j.icarus.2007.12.006

Barnes, J. W., Buratti, B. J., Turtle, E. P., Bow, J., Dalba, P. A., Perry, J., et al. (2013). Precipitation-induced surface brightenings seen on Titan by Cassini VIMS and ISS. *Planetary Science*, *2*, 1. https://doi.org/10.1186/2191-2521-2-1

Barnes, J. W., Lorenz, R. D., Radebaugh, J., Hayes, A. G., Arnold, K., & Chandler, C. (2015). Production and global transport of Titan's sand and particles. *Planetary Science*, *4*, 1. https://doi.org/10.1186/s13535-015-0004-y

Barnes, J. W., Turtle, E. P., Trainer, M. G., Lorenz, R. D., MacKenzie, S. M., Brinckerhoff, W. B., et al. (2021). Science goals and objectives for the Dragonfly Titan rotorcraft relocatable lander. *The Planetary Science Journal*, *2*(4). https://doi.org/10.3847/PSJ/abfdcf

Birch, S. P. D., Hayes, A. G., Howard, A. D., Moore, J. M., & Radebaugh, J. (2016). Alluvial fan morphology, distribution and formation on Titan. *Icarus*, *270*, 238–247. https://doi.org/10.1016/j.icarus.2016.02.013

Bonnefoy, L. E., Hayes, A. G., Hayne, P. O., Malaska, M. J., Le Gall, A., Solominodou, A., & Lucas, A. (2016). Compositional and spatial variations in Titan dune and interdune regions from Cassini VIMS and RADAR. *Icarus*, *270*, 222–237. https://doi.org/10.1016/j.icarus.2015.09.014

Burr, D. M., Bridges, N. T., Marshall, J. R., Smith, J. K., White, B. R., & Emery, J. P. (2015). Higher-than-predicted saltation threshold wind speeds on Titan. *Nature*, *517*, 60–63. https://doi.org/10.1038/nature14088

Burr, D. M., Drummond, S. A., Cartwright, R., Black, B. A., & Perron, J. T. (2013). Morphology of fluvial networks on Titan: Evidence for structural control. *Icarus*, *226*(1), 742–759. https://doi.org/10.1016/j.icarus.2013.06.016

Burr, D. M., Emery, J. P., Lorenz, R. D., Collins, G. C., & Carling, P. A. (2006). Sediment transport by liquid surficial flow: Application to Titan. *Icarus*, *181*(1), 235–242. https://doi.org/10.1016/j.icarus.2005.11.012

Busch, B. (2020). Pilot study on the provenance and depositional controls on clay mineral coatings in active fluvio-eolian systems, Western USA. *Sedimentary Geology*, *406*, 105721. https://doi.org/10.1016/j.sedgeo.2020.105721

Charnay, B., Barth, E., Rafkin, S., Narteau, C., Lebonnois, S., Rodriguez, S., et al. (2015). Methane storms as a driver of Titan's dune orientation. *Nature Geoscience*, *8*, 362–366. https://doi.org/10.1038/ngeo2406

Comola, F., Kok, J. F., Chamecki, M., & Martin, R. L. (2019). The intermittency of wind-driven sand transport. *Geophysical Research Letters*, *46*(22), 13430–13440. https://doi.org/10.1029/2019GL085739

Comola, F., Kok, J. F., Lora, J. M., Cohanim, K., Yu, X., He, C., et al. (2022). Titan's prevailing circulation might drive highly intermittent, yet significant sediment transport. *Geophysical Research Letters*, *49*(7). https://doi.org/10.1029/2022GL097913

Corlies, P., Hayes, A. G., Birch, S. P. D., Lorenz, R., Stiles, B. W., Kirk, R., et al. (2017). Titan's topography and shape at the end of the Cassini mission. *Geophysical Research Letters*, *44*(23), 11754–11761. https://doi.org/10.1002/2017GL075518

Daudon, C., Lucas, A., Rodriguez, S., Jacquemoud, S., Escalante López, A., Grieger, B., et al. (2020). A new digital terrain model of the Huygens landing site on Saturn's largest moon, Titan. *Earth and Space Science*, *7*(12), e2020EA001127. https://doi.org/10.1029/2020EA001127

Davis, R. H., Seravssol, J.-M., & Hinch, E. J. (1986). The elastohydrodynamic collision of two spheres. *Journal of Fluid Mechanics*, *163*, 479–497. https://doi.org/10.1017/s0022112086002392

Dickson, J. L., Lamb, M. P., Williams, R. M. E., Hayden, A. T., & Fischer, W. W. (2020). The global distribution of depositional rivers on early Mars. *Geology*, *49*(5), 504–509. https://doi.org/10.1130/G48457.1

Dietrich, W. E. (1982). Settling velocity of natural particles. *Water Resources Research*, *18*(6), 1615–1626. https://doi.org/10.1029/wr018i006p01615

Edgett, K. S., Banham, S. G., Bennett, K. A., Edgar, L. A., Edwards, C. S., Fairen, A. G., et al. (2020). Extraformational sediment recycling on Mars. *Geosphere*, *16*, 1508–1537. https://doi.org/10.1130/GES02244.1

Ewing, R. C., Hayes, A. G., & Lucas, A. (2015). Sand dune patterns on Titan controlled by long-term climate cycles. *Nature Geoscience*, *8*, 15–19. https://doi.org/10.1038/ngeo2323

Goosmann, E. A., Catling, D. C., Som, S. M., Altermann, W., & Buick, R. (2018). Eolianite grain size distributions as a proxy for large changes in planetary atmospheric density. *Journal of Geophysical Research: Planets*, *123*(10), 2506–2526. https://doi.org/10.1029/2018JE005723

Hayes, A. G. (2016). The lakes and seas of Titan. *Annual Review of Earth and Planetary Sciences*, *44*, 57–83. https://doi.org/10.1146/annurev-earth-060115-012247

Hayes, A. G., Lorenz, R. D., & Lunine, J. I. (2018). A post-Cassini view of Titan's methane-based hydrologic cycle. *Nature Geoscience*, *11*, 306–313. https://doi.org/10.1038/s41561-018-0103-y

Herring, C. (1950). Effect of change of scale on sintering phenomena. *Journal of Applied Physics*, *21*, 301–303. https://doi.org/10.1063/1.1699658

Hörst, S. M. (2017). Titan's atmosphere and climate. *Journal of Geophysical Research: Planets*, *122*, 432–482. https://doi.org/10.1002/2016JE005240

Jerolmack, D. J., Reitz, M. D., & Martin, R. L. (2011). Sorting out abrasion in a gypsum dune field. *Journal of Geophysical Research*, *116*(F2), F02003. https://doi.org/10.1029/2010JF001821

Joseph, G. G., Zenit, R., Hunt, M. L., & Rosenwinkel, A. M. (2001). Particle-wall collisions in a viscous fluid. *Journal of Fluid Mechanics*, *433*, 329–346. https://doi.org/10.1017/S0022112001003470

Kok, J. F., Partelli, E. J. R., Michaels, T. I., & Bou Karam, D. (2012). The physics of wind-blown sand and dust. *Reports on Progress in Physics*, *75*(10), 106901. https://doi.org/10.1088/0034-4885/75/10/106901

Komar, P. D. (2007). The entrainment, transport and sorting of heavy minerals by waves and currents. *Developments in Sedimentology*, *58*, 3–48. https://doi.org/10.1016/S0070-4571(07)58001-5

Lamb, M. P., Dietrich, W. E., & Sklar, L. S. (2008). A model for fluvial bedrock incision by impacting suspended and bed load sediment. *Journal of Geophysical Research*, *113*(E3), F03025. https://doi.org/10.1029/2007JF000915

Lancaster, N. (1982). Dunes of the Skeleton Coast, Namibia (South West Africa): Geomorphology and grain size relationships. *Earth Surface Processes and Landforms*, *7*(6), 575–587. https://doi.org/10.1002/esp.3290070606

Langhans, M. H., Jaumann, R., Stephan, K., Brown, R. H., Buratti, B. J., Clark, et al. (2012). Titan's fluvial valleys: Morphology, distribution, and spectral properties. *Planetary and Space Science*, *60*(1), 34–51. https://doi.org/10.1016/j.pss.2011.01.020

Lapôtre, M. G. A., & Rampe, E. B. (2018). Curiosity's investigation of the Bagnold Dunes, Gale crater: Overview of the two-phase scientific campaign and introduction to the special collection. *Geophysical Research Letters*, *45*(19), 10200–10210. https://doi.org/10.1029/2018GL079032

Le Gall, A., Janssen, M. A., Paillou, P., Lorenz, R. D., Wall, S. D., & the Cassini Radar Team (2010). Radar-bright channels on Titan. *Icarus*, *207*(2), 948–958. https://doi.org/10.1016/j.icarus.2009.12.027

Lopes, R. M. C., Malaska, M. J., Schoenfeld, A. M., Solominodou, A., Birch, S. P. D., Florence, M., et al. (2020). A global geomorphologic map of Saturn's moon Titan. *Nature Astronomy*, *4*, 228–233. https://doi.org/10.1038/s41550-019-0917-6

Lorenz, R. D. (2017). Physics of saltation and sand transport on Titan: A brief review. *Icarus*, *230*, 162–167. https://doi.org/10.1016/j.icarus.2013.06.023

Lorenz, R. D., & Lunine, J. I. (1996). Erosion on Titan: Past and present. *Icarus*, *122*(1), 79–91. https://doi.org/10.1006/icar.1996.0110

Lorenz, R. D., MacKenzie, S. M., Neish, C. D., Le Gall, A., Turtle, E. P., Barnes, J. W., et al. (2021). Selection and characteristics of the Dragonfly landing site near Selk crater, Titan. *The Planetary Science Journal*, *2*(1), 24. https://doi.org/10.3847/PSJ/abd08f

Lorenz, R. D., Niemann, H. B., Harpold, D. N., Way, S. H., & Zarnecki, J. C. (2006). Titan's damp ground: Constraints on Titan surface thermal properties from the temperature evolution of the Huygens GCMS inlet. *Meteoritics & Planetary Sciences*, *41*(11), 1705–1714. https://doi.org/10.1111/j.1945-5100.2006.tb00446.x

Lorenz, R. D., Wall, S., Radebaugh, J., Boubin, G., Reffet, E., Janssen, M., et al. (2006). The sand seas of Titan: Cassini RADAR observations of longitudinal dunes. *Science*, *312*(5774), 724–727. https://doi.org/10.1126/science.1123257

Malaska, M. J., Hodyss, R., Lunine, J. I., Hayes, A. G., Hofgartner, J. D., Hollyday, G., et al. (2017). Laboratory measurements of nitrogen dissolution in Titan lake fluids. *Icarus*, *289*, 94–105. https://doi.org/10.1016/j.icarus.2017.01.033

Malaska, M. J., Lopes, R. M. C., Hayes, A. G., Radebaugh, J., Lorenz, R. D., & Turtle, E. P. (2016). Material transport map of Titan: The fate of dunes. *Icarus*, *270*, 183–196. https://doi.org/10.1016/j.icarus.2015.09.029

Malaska, M. J., Lopes, R. M. C., Williams, D. A., Neish, C. D., Solomonodou, A., Soderblom, J. M., et al. (2016). Geomorphological map of the Afekan Crater region, Titan: Terrain relationships in the equatorial and mid-latitude regions. *Icarus*, *270*, 130–161. https://doi.org/10.1016/j.icarus.2016.02.021

Malaska, M. J., Radebaugh, J., Lopes, R. M. C., Mitchell, K. L., Verlander, T., Schoenfeld, A. M., et al. (2020). Labyrinth terrain on Titan. *Icarus*, *344*, 113764. https://doi.org/10.1016/j.icarus.2020.113764

Mendéz Harper, J. S., McDonald, G. D., Dufek, J., Malaska, M. J., Burr, D. M., Hayes, A. G., et al.(2017). Electrification of sand on Titan and its influence on sediment transport. *Nature Geoscience*, *10*, 260–265. https://doi.org/10.1038/ngeo2921

Neish, C. D., Barnes, J. W., Sotin, C., MacKenzie, S., Soderblom, J. M., Le Mouélic, S., et al. (2015). Spectral properties of Titan's impact craters imply chemical weathering of its surface. *Geophysical Research Letters*, *42*(10), 3746–3754. https://doi.org/10.1002/2015GL063824

Parker, G. (1991). Selective sorting and abrasion of river gravel. I: Theory. *Journal of Hydraulic Engineering*, *117*(2), 131–147. https://doi.org/10.1061/(asce)0733-9429(1991)117:2(131)

Pastore, G., Baird, T., Vermeesch, P., Bristow, C., Resentini, A., & Garzanti, E. (2021). Provenance and recycling of Sahara Desert sand. *Earth-Science Reviews*, *216*, 103606. https://doi.org/10.1016/j.earscirev.2021.103606

Perron, J. T., Lamb, M. P., Koven, C. E., Fung, I. Y., Yager, E., & Ádámkovics, M. (2006). Valley formation and methane precipitation rates on Titan. *Journal of Geophysical Research*, *111*(E11), E11001. https://doi.org/10.1029/2005JE002602

Poggiali, V., Mastrogiuseppe, M., Hayes, A. G., Seu, R., Birch, S. P. D., Lorenz, R., et al. (2016). Liquid-filled canyons on Titan. *Geophysical Research Letters*, *43*(15), 7887–7894. https://doi.org/10.1002/2016GL069679

Rodriguez, S., Le Mouélic, S., Barnes, J. W., Kok, J. F., Rafkin, S. C. R., Lorenz, R. D., et al. (2018). Observational evidence for active dust storms on Titan at equinox. *Nature Geoscience*, *11*, 727–732. https://doi.org/10.1038/s41561-018-0233-2

Scheingross, J. S., Brun, F., Lo, D. Y., Omerdin, K., & Lamb, M. P. (2014). Experimental evidence for fluvial bedrock incision by suspended and bedload sediment. *Geology*, *42*(6), 523–526. https://doi.org/10.1130/G35432.1

Sklar, L. S., & Dietrich, W. E. (2001). Sediment and rock strength controls on river incision into bedrock. *Geology*, *29*(12), 1087–1090. https://doi.org/10.1130/0091-7613(2001)029<1087:SARSCO>2.0.CO;2

Sklar, L. S., & Dietrich, W. E. (2004). A mechanistic model for river incision into bedrock by saltating bed load. *Water Resources Research*, *40*(6), W06301. https://doi.org/10.1029/2003WR002496

Solomonodou, A., Coustenis, A., Lopes, R. M. C., Malaska, M. J., Rodriguez, S., Drossart, P., et al. (2018). The spectral nature of Titan's major geomorphological units: Constraints on surface composition. *Journal of Geophysical Research: Planets*, *123*(2), 489–507. https://doi.org/10.1002/2017JE005477

Tirsch, D., Jaumann, R., Pacifici, A., & Poulet, F. (2011). Dark aeolian sediments in Martian craters: Composition and sources. *Journal of Geophysical Research*, *116*(E3), E03002. https://doi.org/10.1029/2009JE003562

Tokano, T. (2008). Dune-forming winds on Titan and the influence of topography. *Icarus*, *194*(1), 243–262. https://doi.org/10.1016/j.icarus.2007.10.007

Tokano, T. (2010). Relevance of fast westerlies at equinox for the eastward elongation of Titan's dunes. *Aeolian Research*, *2*, 113–127. https://doi.org/10.1016/j.aeolia.2010.04.003

Tomasko, M. G., Archinal, B., Becker, T., Bézard, B., Bushroe, M., Combes, M., et al. (2005). Rain, winds and haze during Huygens probe's descent to Titan's surface. *Nature*, *438*, 765–778. https://doi.org/10.1038/nature04126

Trower, E. J., Lamb, M. P., & Fischer, W. W. (2017). Experimental evidence that ooid size reflects a dynamic equilibrium between rapid precipitation and abrasion rates. *Earth and Planetary Science Letters*, *468*, 112–118. https://doi.org/10.1016/j.epsl.2017.04.004

Turtle, E. P., Perry, J. E., Hayes, A. G., Lorenz, R. D., Barnes, J. W., McEwen, A. S., et al. (2011). Rapid and extensive surface changes near Titan's equator: Evidence of April showers. *Science*, *331*(6023), 1414–1417. https://doi.org/10.1126/science.1201063

Williams, K. E., McKay, C. P., & Persson, F. (2012). The surface energy balance at the Huygens landing site and the moist surface conditions on Titan. *Planetary and Space Science*, *60*(1), 376–385. https://doi.org/10.1016/j.pss.2011.11.005

Yu, X., Hörst, S. M., He, C., McGuiggan, P., & Crawford, B. (2018). Where does Titan sand come from: Insight from mechanical properties of Titan sand candidates. *Journal of Geophysical Research: Planets*, *123*(9), 2310–2321. https://doi.org/10.1029/2018JE005651

Zarnecki, J. C., Leese, M. R., Hathi, B., Ball, A. J., Hagermann, A., Towner, M. C., et al. (2005). A soft solid surface on Titan as revealed by the Huygens surface science package. *Nature*, *438*, 792–795. https://doi.org/10.1038/nature04211

References From the Supporting Information

Engineering ToolBox (2004). *Ice - thermal properties*. Retrieved from https://www.engineeringtoolbox.com/ice-thermal-properties-d_576.html

Hörst, S. M., & Tolbert, M. A. (2013). In situ measurements of the size and density of Titan aerosol analogs. *The Astrophysical Journal*, *770*(1). https://doi.org/10.1088/2041-8205/770/1/L10

Imanaka, H., Cruishank, D. P., Khare, B. N., & McKay, C. P. (2012). Optical constants of Titan tholins at mid-infrared (2.5–25 μm) and the possible chemical nature of Titan's haze particles. *Icarus*, *218*(1), 247–261. https://doi.org/10.1016/j.icarus.2011.11.018

Meyers, M. A., & Chawla, K. K. (2008). *Mechanical behavior of materials*. Cambridge University Press.